

AD A 041 456

AD NO.
DDC FILE COPY

PROPAGATION EFFECTS OF STEEP STRIATIONS

Science Applications, Inc.
1200 Prospect Street
La Jolla, California 92037

30 November 1976

Topical Report for Period 1 November 1975—
30 November 1976

CONTRACT No. DNA 001-75-C-0033

APPROVED FOR PUBLIC RELEASE;
DISTRIBUTION UNLIMITED.

THIS WORK SPONSORED BY THE DEFENSE NUCLEAR AGENCY
UNDER RDT&E RMSS CODE 8322075464 S99QAXHB05401 H2590D.

Prepared for
Director
DEFENSE NUCLEAR AGENCY
Washington, D. C. 20305

DNA 4170T

12

DEC 1 1976
D F O

Destroy this report when it is no longer
needed. Do not return to sender.



UNCLASSIFIED

SECURITY CLASSIFICATION OF THIS PAGE (When Data Entered)

REPORT DOCUMENTATION PAGE		READ INSTRUCTIONS BEFORE COMPLETING FORM	
1. REPORT NUMBER DNA 417DT	2. GOVT ACCESSION NO.	3. RECIPIENT'S CATALOG NUMBER	
4. TITLE (and Subtitle) PROPAGATION EFFECTS OF STEEP STRIATIONS,		5. TYPE OF REPORT & PERIOD COVERED Topical Report for Period 1 Nov 75-30 Nov 76,	
7. AUTHOR(s) David L./Sachs		6. PERFORMING ORG. REPORT NUMBER SAI-76-847-LJ	
9. PERFORMING ORGANIZATION NAME AND ADDRESS Science Applications, Inc. 1200 Prospect Street La Jolla, California 92037		8. CONTRACT OR GRANT NUMBER(s) DNA 001-75-C-0033	
11. CONTROLLING OFFICE NAME AND ADDRESS Director Defense Nuclear Agency Washington, D.C. 20305		10. PROGRAM ELEMENT, PROJECT, TASK AREA & WORK UNIT NUMBERS NWED Subtask S99QAXHBQ54-01	
14. MONITORING AGENCY NAME & ADDRESS (if different from Controlling Office) 123456789		12. REPORT DATE 30 November 1976	
		13. NUMBER OF PAGES 42	
		15. SECURITY CLASS (of this report) UNCLASSIFIED	
		15a. DECLASSIFICATION DOWNGRADING SCHEDULE	
16. DISTRIBUTION STATEMENT (of this Report) Approved for public release; distribution unlimited.			
17. DISTRIBUTION STATEMENT (of the abstract entered in Block 20, if different from Report)			
18. SUPPLEMENTARY NOTES This work sponsored by the Defense Nuclear Agency under RDT&E RMSS Code B322075464 S99QAXHBQ5401 H2590D.			
19. KEY WORDS (Continue on reverse side if necessary and identify by block number) Radio Scintillation Striations			
20. ABSTRACT (Continue on reverse side if necessary and identify by block number) This report describes the fluctuations in intensity that occur when a radio signal traverses striated ionization. The difference in the severity of the effects for steep and gentle striation edges is shown to be a function of the product of signal wavelength and distance from the striations.			

DD FORM 1 JAN 73 1473

EDITION OF 1 NOV 65 IS OBSOLETE

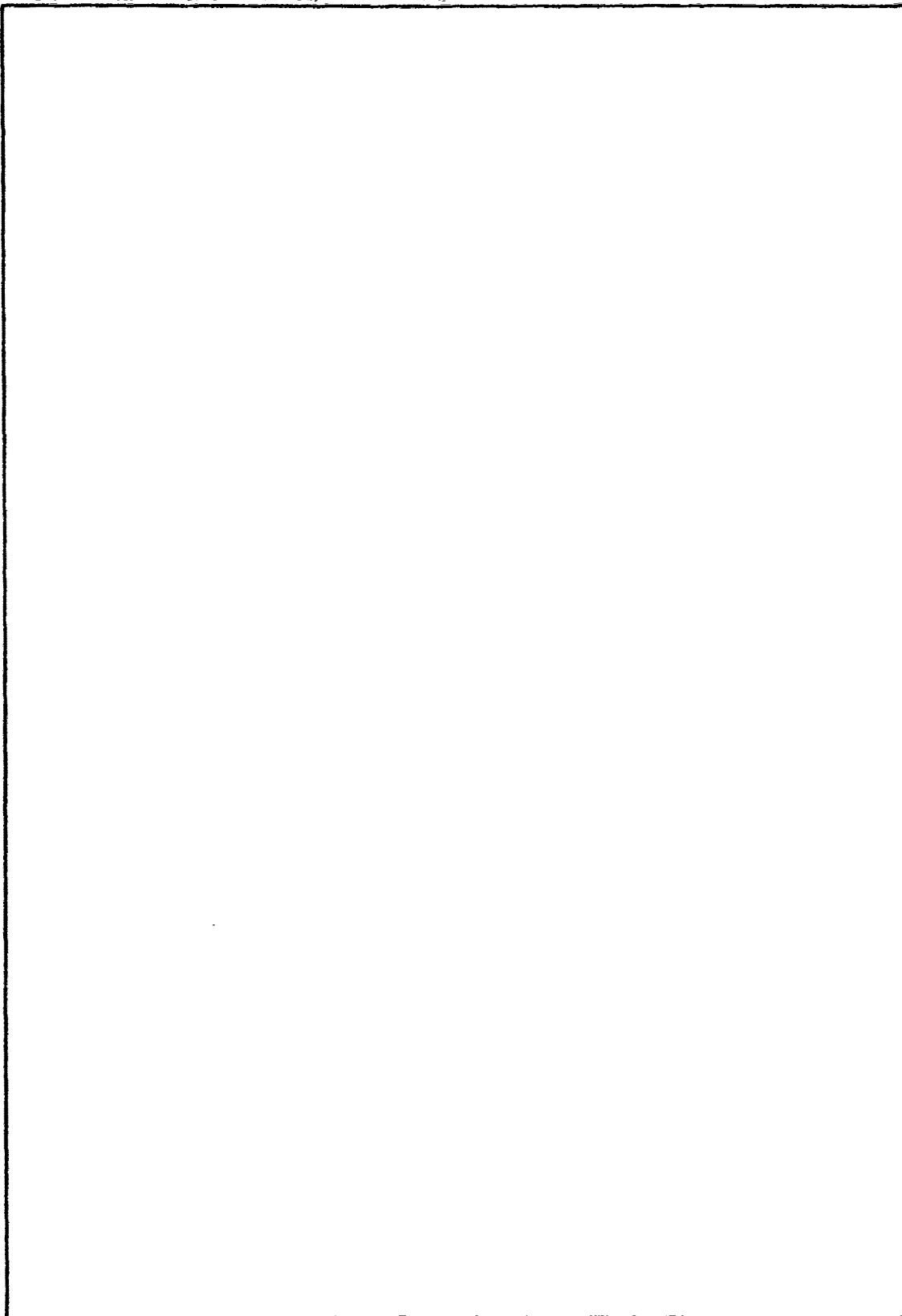
UNCLASSIFIED

SECURITY CLASSIFICATION OF THIS PAGE (When Data Entered)

388 Y62

UNCLASSIFIED

SECURITY CLASSIFICATION OF THIS PAGE(When Data Entered)



UNCLASSIFIED

SECURITY CLASSIFICATION OF THIS PAGE(When Data Entered)

TABLE OF CONTENTS

	<u>Page</u>
1. INTRODUCTION AND SUMMARY	3
2. ANALYTIC METHODS	7
2.1 Analysis.	7
2.2 Implementation.	21
3. RESULTS.	25
REFERENCES.	35

ACCESSION No.	
RTIS	Write Section <input checked="" type="checkbox"/>
BDC	Write Section <input type="checkbox"/>
UNANNOUNCED	<input type="checkbox"/>
JUSTIFICATION	
BY	
FILE CODES	
DATE	

A

DECEMBER
JULY
RECEIVED

ILLUSTRATIONS

	<u>Page</u>
1. Specific and Average Power Spectra Gaussian Profile.	11
2. Specific and Average Power Spectra Rod Profile	12
3. Average Bit Error Probability Versus rms Phase Fluctuation for Noncoherent FSK Modulation and 15dB Average Signal-to- Noise Ratio.	29
4. Contours of Bit Error Probability.	30
5. Contours of S_4 ; Gaussian	31
6. Contours of S_4 ; Rod.	32
7. Contours for 1% Probability of Fades > 12dB.	34

1. INTRODUCTION AND SUMMARY

This report describes the fluctuations in intensity that occur when a radio signal traverses striated ionization. The ionization is modeled as a collection of cylinders of electron density randomly positioned in space. This work is a continuation of a previous analysis¹. The major improvements on that analysis are:

1. The use of fast Fourier transforms to calculate the signal a distance d , beyond the ionization instead of the method of rays and caustics used previously.
2. The analysis is carried out for two extreme profiles of striation electron density; the Gaussian profile previously studied and a rod profile representing an extreme steepening of the striation edge.
3. Results of systems significance are presented graphically as contours on a λd versus $\Delta\phi_{\text{rms}}$ plot where λ is the signal wavelength and $\Delta\phi_{\text{rms}}$ is the root-mean-square signal phase variation directly produced by the ionization.

The last improvement allows the difference between the extreme profiles' effects to be easily seen as a function of the parameters λd and $\Delta\phi_{\text{rms}}$.

The set of striations used is the same as that used previously¹, a set of 210 striations set randomly in an area 64 km wide by a thickness T . The thickness does not enter the calculations since we use the thin-screen approximation. This approximation, whose validity criteria were previously derived¹ for Gaussian profiles, is adequate to demonstrate the propagation effects for the striations considered in this report. We do not foresee any qualitative changes by its removal and intend to demonstrate this in future works.

We find the rod and Gaussian profiles to produce similar propagation effects for $\lambda d > 3 \text{ km}^2$ where the dependence on λd is weakening. In the high λd regime, amplitude scintillation onsets at $\Delta\phi_{\text{rms}} \approx 0.3$ radians. As λd becomes smaller the rod and Gaussian profile effects diverge with onset for Gaussian effects occurring at

$$\Delta\phi_{\text{rms}} = \frac{1}{\lambda d}$$

whereas

$$\Delta\phi_{\text{rms}} = \frac{1}{\sqrt{3\lambda d}}$$

for the onset of rod effects.

Thus the profile shape is relatively unimportant at UHF ($\lambda \sim 10^{-3} \text{ km}$), but becomes very important at K Band ($\lambda \sim 10^{-5} \text{ km}$). We assume $10^2 < d < 10^4 \text{ km}$ for typical situations. For $d = 10^3$ and K Band the Gaussian profile effects onset

$$\text{at } \Delta\phi_{\text{rms}} = 100 \text{ radians}$$

while the rod profile effects onset

$$\text{at } \Delta\phi_{\text{rms}} = 6 \text{ radians.}$$

The rms phase is given by

$$\Delta\phi_{\text{rms}} = 2.818 \cdot 10^{-3\lambda} n_0 Q_{\text{rms}}$$

where n_0 is the striation on-axis electron density (cm^{-3}) and Q is the normalized

integrated electron density. For the particular set of striations used, $Q_{rms} = 2.07$ km for the Gaussian profile and $Q_{rms} = 2.55$ km for the rod profile. This indicates $\Delta\phi_{rms}$ to be relatively insensitive to profile shape for a given set of striations and values of n_0 and λ . However, the value of $\Delta\phi_{rms}$ required for the onset of degradation is highly sensitive to profile when $\lambda d < 3 \text{ km}^2$. The set of striations we have used have sizes ranging from 323m to 1614m with a maximum number at 775m. One can scale our results to different sizes by changing each size a to δa and scaling λz as δ^{-2} . The size distribution used is a discrete approximation to the continuous Chesnut distribution which gives the analytic formula for Gaussian profiles

$$Q_{rms}^2 = \frac{\sqrt{8}}{3} \pi a_0^3 \left(\frac{M}{L}\right)$$

where a_0 is a characteristic size of the distribution (~ 0.76 km for the set used), M is the total number of striations imbedded in an area $L \times T$. Since T does not matter, if we scale a_0 and L to δa_0 and δL , Q_{rms} scales as δ .

This study has contrasted the propagation effects of smooth versus abrupt profiles for a set of striations. The abrupt profiles produce more severe propagation effects than smooth profiles at high frequencies. Future work will address this question for other sets of striation sizes. We do not foresee other sets of striations producing effects more severe than were found here for the abrupt profiles. We illustrate this statement with an example. Suppose we are at the threshold of rod effects at $\lambda d = 0.1$ and $\Delta\phi_{rms} = \sqrt{10}$. If we change the sizes of all striations by dividing them and the width L by $\sqrt{10}$ we effectively have changed λd to 1 and $\Delta\phi_{rms}$ to 1 which keeps us at the threshold of rod-effects (Gaussian effects get worse). If we continued to

divide the sizes we would reach $\Delta\phi_{rms} < 0.3$ and propagation effects would cease. We believe the results presented in this report for rod profiles constitute a reasonable upper bound for estimates of system degradation effects in terms of $\Delta\phi_{rms}$ and λd .

2. ANALYTIC METHODS

2.1 ANALYSIS

We use the thin-screen approximation to describe the signal which results after a plane wave propagates through a region of striated ionization. The derivation and validity criteria of this approximation are in reference 1. The ionization is represented by a collection of striations each of which has a profile of electron density

$$n_e(\vec{x}) = n_i(\vec{x} - \vec{x}_i, a_i)$$

where $\vec{x}_i = (x_i, z_i)$ is the two dimensional position of the i 'th striation and a_i is its characteristic size. The electron density is uniform in the third dimension.

For a plane wave propagating in the z direction, the thin-screen approximation describes the effect of each striation on the signal to be a phase change

$$\phi_i(x - x_i, a_i) = \int n_i(\vec{x} - \vec{x}_i, a_i) dz \frac{k_0}{2n_c}$$

where k_0 is the wave number of the signal $= 2\pi/\lambda$ where λ is the wavelength and $n_c = k_0^2/4\pi r_e$, the critical electron density where $r_e = 2.818 \cdot 10^{-13}$ cm, the electron classical radius. The total effect on the signal is then a net phase change due to all the striations of

$$\phi(x) = \sum_i \phi_i(x - x_i, a_i) .$$

We consider two extremes of electron density profile:

$$\text{The Gaussian, } n_i^g = n_0 e^{-(\vec{x} - \vec{x}_i)^2 / a_i^2}$$

which produces the phase

$$\phi_i^g = C \sqrt{\pi} a_i e^{-(x - x_i)^2 / a_i^2};$$

$$\begin{aligned} \text{the rod, } n_i^r &= n_0 \quad |\vec{x} - \vec{x}_i| < a_i \\ &= 0 \quad |\vec{x} - \vec{x}_i| > a_i \end{aligned}$$

which produces the phase

$$\phi_i^r = C 2a_i \sqrt{1 - \frac{(x - x_i)^2}{a_i^2}}$$

$$\text{where } C = \frac{k_0 n_0}{2n_c} = r_e \lambda n_0.$$

The actual profile of a striation should fall between these two extremes.

The total phase has the Fourier transform

$$\begin{aligned} F(v) &= \int dx e^{-i2\pi vx} \phi(x) \\ &= \sum_i e^{-i2\pi vx_i} F_i(v) \end{aligned}$$

$$\text{where } F_i^g(v) = C \pi a_i^2 e^{-\pi^2 v^2 a_i^2} \text{ and } F_i^r(v) = C \frac{a_i}{v} J_1(2\pi v a_i),$$

where J_1 is a Bessel function.

Notice that $F_i^g(0) = F_i^a(0) = C\pi a_i^2$ because each profile has the same electron content, $\int dx \int dz n_i(\vec{x} - \vec{x}_i, a_i) = \pi n_0 a_i^2$.

For a given set of striations, the phase has a power spectrum

$$P(v) = |F(v)|^2 = \sum_i F_i^2(v) + 2 \sum_{i < j} F_i(v) F_j(v) \cos[2\pi v(x_i - x_j)] .$$

The first term is independent of the positions of the striations. The second term would be larger than the first by about a factor of the total number of the striations if the cosine terms all added coherently. The discussion of the propagation effects of a collection of striations should ideally not be dependent on their particular positioning unless it can be shown that characteristics of their positioning can be predicted by the phenomenology. Since no positioning characteristics have yet come from phenomenology, the second term can be eliminated by considering the striations to be randomly placed and averaging over an ensemble of random placements. If the total area occupied by the striations is small compared to the area they are placed in, one can approximate² the probability of any two striations' placement as independent and equally likely within the area. The position, x_i , is then equally likely on a line, L , which produces an average power spectrum of

$$\overline{P(v)} = \sum_i F_i^2(v) + 2S^2 \sum_{i < j} F_i(v) F_j(v)$$

where $S = \frac{\sin(\pi v L)}{\pi v L}$.

By evaluating the spectrum at values of

$$v_n = \frac{n}{L} \quad n = 1, 2, 3, \dots$$

where $S = 0$, we are correctly ignoring the effects of the finite interval, L , on the Fourier transform. We are expanding $\phi(x)$ in a Fourier series.

The propagation calculations will be performed for one set of random positions of the striations. This is the situation an actual radio signal encounters. We illustrate in Figures 1 and 2 the power spectrum for the one set and the average power spectrum for the Gaussian and rod profiles. The scale is normalized ($C = 1$). We use a set of positions and radii furnished by Dr. W. Chesnut³(SRI). This is his "Type B" distribution consisting of 210 striations whose positions are randomly distributed over a line $L = 64$ km. This distribution was also used in reference 1.

It is obvious that the large differences between the specific set of positions and the average at low- ν is a chance alignment in phases for the positions chosen. It appears for both Gaussian and rod spectra.

The rod spectra have a higher frequency content of course. The spectra appear to change from exponential to power law at $\nu = 1$. Since there are no striations in the set with $a_i < 0.323$ km, all Bessel functions would have arguments greater than 2 for $\nu = 1$. They then decrease with an envelope of $\nu^{-3/2}$, giving the power spectrum a ν^{-3} fall off. The Gaussian spectrum is exponential until $\nu = 1.5$ where the Gaussian fall off should take over

The propagation calculations we will perform with the specific set of striations depend on the Fourier transform of $e^{i\phi(x)}$. We cannot yet analytically determine the effect of the large low- ν variation in the power spectrum of $\phi(x)$ for the specific set on our calculated effects. Our intuition says the low- ν portion of the spectrum is unimportant so long as it is finite. We also feel that all statistical properties of the signal of interest will be unaffected by the noise-like difference between the specific and average spectrum.

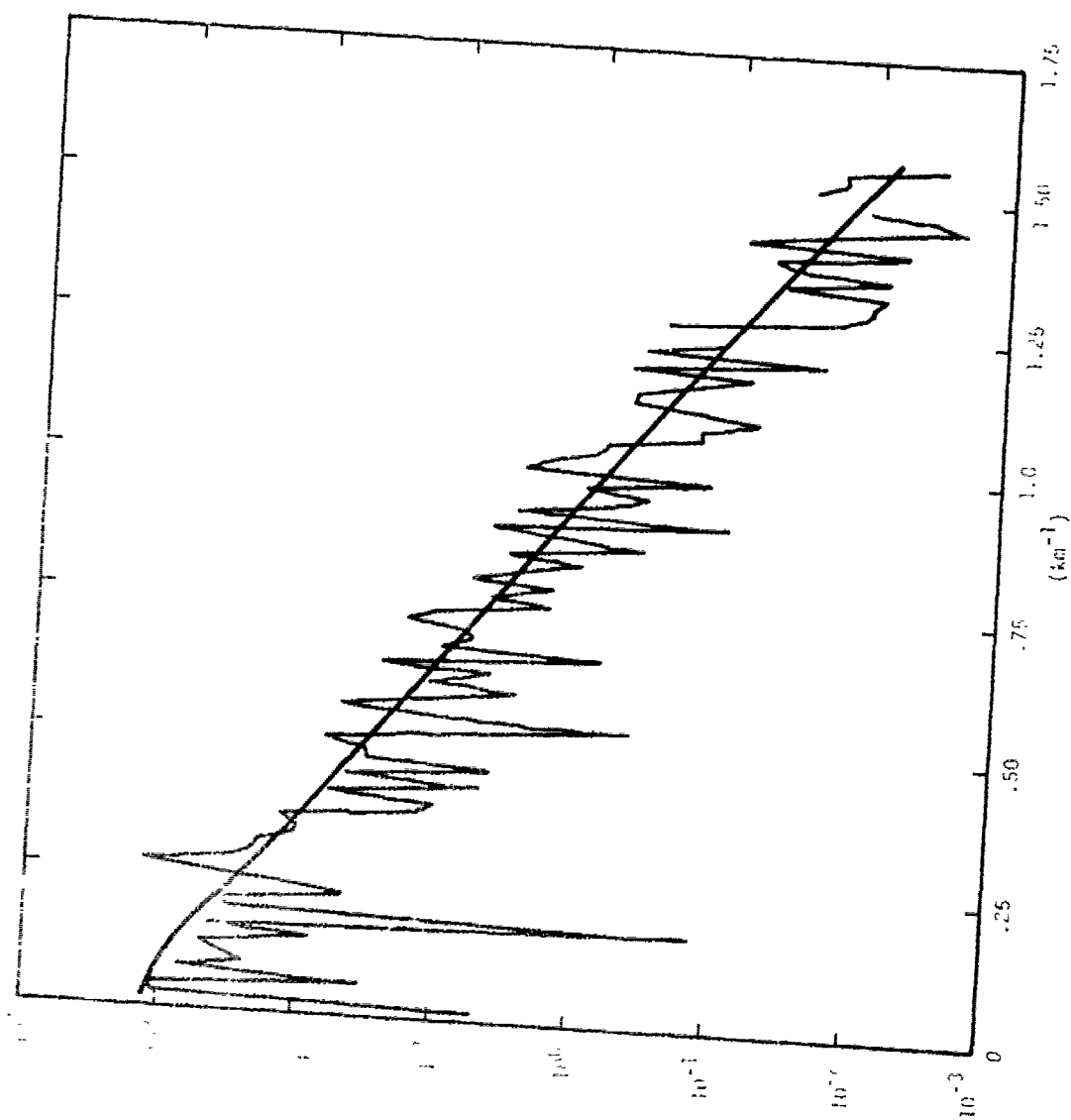


FIGURE 1 - Specific and Average Power Spectra Gaussian Profile

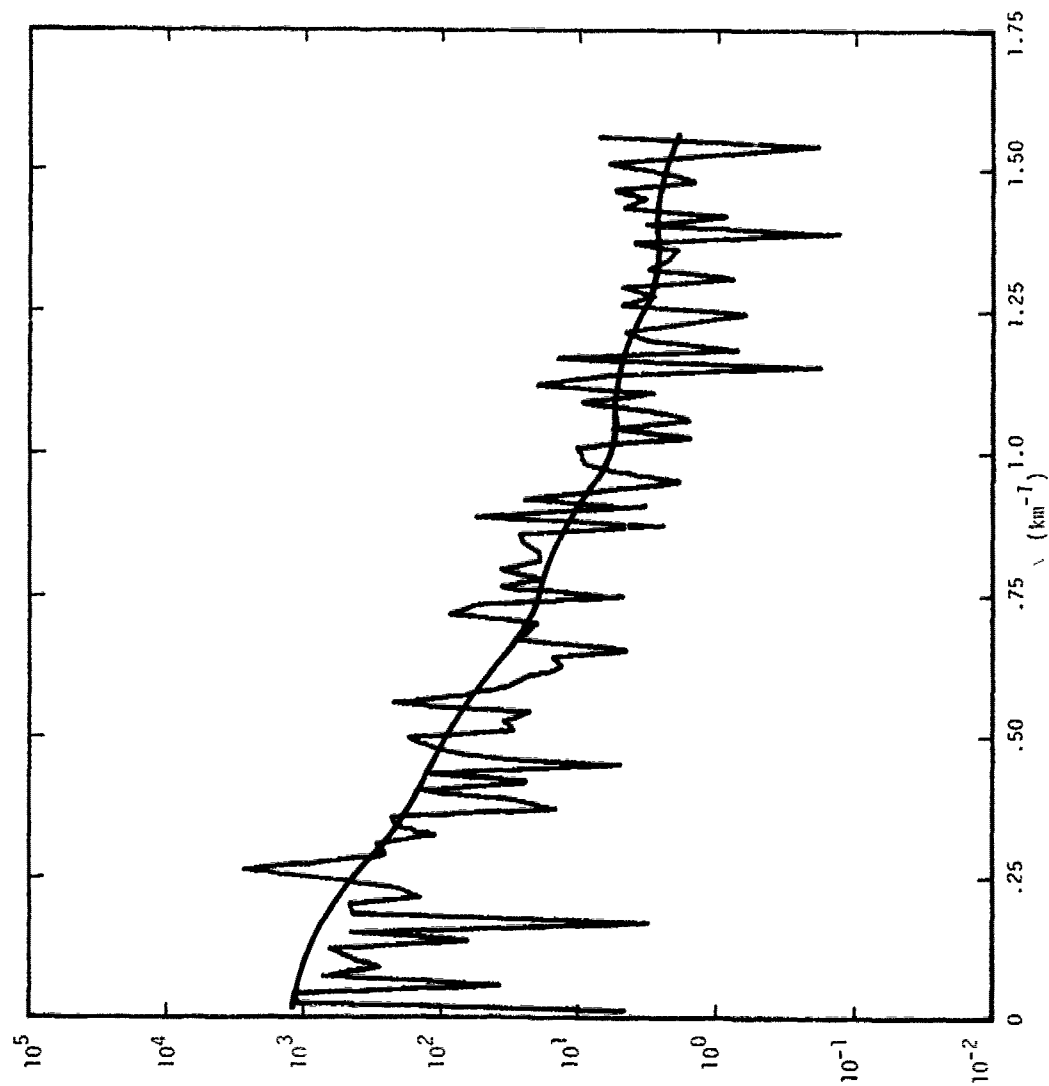


Figure 2 - Specific and Average Power Spectra Rod Profile

Consider the following statistical functions:

$$\bar{\phi} \equiv \frac{1}{L} \int_0^L dx \phi(x) = \frac{F(0)}{L}$$

$$\begin{aligned} \Delta\phi = \phi - \bar{\phi} &= \frac{1}{L} \sum_{n=-\infty}^{\infty} F\left(\frac{n}{L}\right) e^{i2\pi nx/L} - \frac{F(0)}{L} \\ &= \frac{1}{L} \sum_{n=1}^{\infty} \left[F\left(\frac{n}{L}\right) e^{i2\pi nx/L} + F\left(\frac{-n}{L}\right) e^{-i2\pi nx/L} \right] \end{aligned}$$

That is, the Fourier transform of $\Delta\phi$ is the same as the Fourier transform of ϕ with the $v = 0$ term removed. The auto correlation function

$$\begin{aligned} \overline{\Delta\phi(x)\Delta\phi(x+\Delta x)} &\equiv \frac{1}{L} \int_0^L dx \Delta\phi(x)\Delta\phi(x+\Delta x) \\ &= \frac{1}{L^2} \sum_{n=1}^{\infty} P\left(\frac{n}{L}\right) \left[e^{i2\pi n\Delta x/L} + e^{-i2\pi n\Delta x/L} \right] \end{aligned}$$

which follows by substitution and the properties

$$\begin{aligned} \frac{1}{L} \int_0^L dx e^{i2\pi x/L(n+n')} &= 0 \quad n \neq -n' \\ &= 1 \quad n = -n' \end{aligned}$$

$$F\left(\frac{-n}{L}\right) = F^*\left(\frac{n}{L}\right).$$

We have the well known result that the power spectrum is the Fourier transform of the auto correlation function. In this case we are referring to power per unit length since we are interested in $\Delta\phi$ over the interval $(0,L)$ only. Over this interval the auto correlation function is meaningful out to $|\Delta x| = L/2$

since beyond this value the periodicity of $\Delta\phi$ causes it to mirror its behavior back to its value at $\Delta x = 0$. That is, $\overline{\Delta\phi(x)\Delta\phi(x+L-\Delta x)} = \overline{\Delta\phi(x)\Delta\phi(x+\Delta x)}$.

Indeed, for cases of interest to be treated later, $\overline{\Delta\phi^2} = \frac{2}{L^2} \sum_n P(\frac{n}{L}) \gg 1$. This causes most of the interest in the auto correlation function to be in its behavior at small Δx . For example, one item of interest is that value of Δx where

$$\overline{\Delta\phi\Delta\phi(\Delta x)} - \overline{\Delta\phi^2} = -1 \quad \text{or}$$

$$\frac{2}{L^2} \sum_n P(\frac{n}{L}) [1 - \cos(2\pi \frac{n\Delta x}{L})] = 1 \quad \text{or}$$

$$\frac{4}{L^2} \sum_n P(\frac{n}{L}) \sin^2(\frac{n\Delta x}{L}) = 1 .$$

Since this will occur at a value of $\Delta x \ll L$, the low v (small n) difference between the specific and average spectrum should not impact the result. Similarly for $\pi\Delta x \ll L$, the \sin^2 weighting will vary slowly over a range of n values which smoothes out the differences between the specific and average spectrum.

The discrete distribution of a_i that we use approximates the continuous Chesnut distribution,

$$m(a)da = \frac{8M}{3\sqrt{\pi}} \frac{a_0^5}{a^6} e^{-(a_0^2/a^2)} da ,$$

the number of striations of size a in an interval da . The total number of striations, $M = 210$.

Analytically,

$$\begin{aligned} \overline{P(v)} &= \int_0^{\infty} \ln(a) da \left(C \pi a^2 e^{-\pi^2 v^2 a^2} \right)^2 \\ &= \frac{4}{3} C^2 \pi^2 a_0^4 M e^{-\sqrt{8} \pi v a_0} \end{aligned}$$

for the Gaussian profile.

Figure 1 shows the exponential behavior quite well except near $v = 0$ where the cutoff of large striations in the discrete distribution returns the vanishing slope at the origin. From Figure 1, a measured slope of 7.83 produces the value $a_0 = 0.881$ km.

We are interested in relating the propagation effects to a characteristic size of the distribution used and to the parameter

$$\overline{\Delta \phi^2} = \frac{2}{L^2} \sum_n P\left(\frac{n}{L}\right) = \frac{2}{L} \int_0^{\infty} P(v) dv = \frac{\sqrt{8}}{3} C^2 \pi a_0^3 \left(\frac{M}{L}\right)$$

for the continuous distribution. We have measured this quantity directly from the discrete distribution and find

$$\Delta \phi_{rms} = \sqrt{\overline{\Delta \phi^2}} = 2.0711 C .$$

Substitution of this value into the above equation produces $a_0 = 0.761$ km. Thus there is a 10% discrepancy in determining a_0 from specific and average discrete distributions using formulas for a continuous distribution. Since the geometric structure of the striations we use is fixed, we will relate the propagation effects to $\Delta \phi_{rms}$ by variations of the parameter C .

We now discuss the signal at a distance d beyond the striated region.
If the signal is defined as

$$E = U(x,z)e^{i(k_0 z - \omega t)}$$

and $U(x,0) = e^{i\phi(x)}$ at the exit plane of the striations, the signal at some point (x_0, d) beyond the exit plane is obtained from the free-space parabolic equation

$$\frac{\partial U}{\partial z} + \frac{1}{2ik_0} \frac{\partial^2 U}{\partial x^2} = 0.$$

Fourier analysis of the parabolic equation shows that for

$$U(x,0) = \sum_k \hat{U}(k) e^{ikx}$$

$$U(x_0, d) = \sum_k \hat{U}(k) e^{i[kx_0 - \frac{k^2 d}{2k_0}]}$$

This method has had widespread use by workers in striation propagation and is efficient for production runs of $U(x_0, d)$ because of fast Fourier transform techniques. This technique decomposes the signal at $z = 0$ into plane waves, propagates each plane wave to the receiver at (x_0, d) and sums the waves to obtain $U(x_0, d)$. Since $U(x,0)$ was defined only for $0 < x < L$, the use of a sum (Fourier series) rather than an integral specifies $U(x,0)$ as periodic in L . We can accept this as an unimportant consequence so long as we do not evaluate the signal at values of d so far from the screen that the signal is influenced by values of $U(x,0)$ over an interval greater than L .

The Fresnel distance for an interval L is

$$d_f = k_0 L^2 / 2 .$$

The smallest wave number of interest is $\sim 5 \cdot 10^3 \text{ km}^{-1}$ so we need $d < d_f \approx 10^7 \text{ km}$ for $L = 64 \text{ km}$, which is well satisfied for cases of interest. A further requirement when large phase variations occur is $L/2d > \theta_M$ where θ_M is the largest angle of a significantly contributing plane wave.

The parabolic equation is a small angle approximation to the wave equation. For each plane wave, the parameter k is $k_0 \sin \theta_k \approx k_0 \theta_k$. The amplitude of the plane wave is the Fourier integral

$$\hat{U}(k) = \frac{1}{L} \int_0^L e^{i[\phi(x) - kx]} dx$$

As in a previous analysis¹, we may define a local phase-front angle

$$\theta(x) = \frac{1}{k_0} \frac{\partial \phi}{\partial x}$$

and the integral is

$$\hat{U}(k) = \frac{1}{L} \int_0^L e^{ik_0 \int_0^x (\phi(x') - \theta_k) dx'} dx$$

If instead of fast Fourier techniques, we evaluated the integral by stationary phase¹, the points of stationary phase would be wherever

$$\theta(x_s) = \theta_k$$

and

$$\hat{U}(k) = \sqrt{\frac{2\pi i}{L_0^2 k_0}} \sum_s \frac{e^{i[\phi_0(x_s) - kx_s]}}{\sqrt{\theta'(x_s)}}$$

with a criterion for the validity of this method of $|\theta''(x_s)|^2 \ll k_0 |\theta'(x_s)|^3$.

Although this method of evaluation of the integral becomes inaccurate where $\theta'(x)$ is small, it is clear that there are negligible contributions to the integral for $\theta_k > \theta(x)_{\max}$ since there would then be no stationary points.

For a Gaussian profile

$$\theta_i(x) = \frac{-2C\pi}{k_0 a_i} (x-x_i) e^{-(x-x_i)^2/a_i^2}$$

with maximum value

$$\theta_{i_{\max}} = \sqrt{\frac{2\pi}{e}} \frac{C}{k_0} = \sqrt{\frac{\pi}{2e}} \frac{n_0}{n_c} \ll 1$$

and depending on the number of striations along the path there is some finite limit of θ_k for which the requirement

$$d < \frac{L}{2\theta_M}$$

can be tested.

For the case of a rod profile

$$\theta_i(x) = \frac{-C}{k_0 a_i} \frac{(x-x_i)}{\sqrt{1 - \frac{(x-x_i)^2}{a_i^2}}}$$

which approaches infinity as $|(x-x_i)|$ approaches a_i and there is no limit on $\theta(x)$. Indeed there are two infinities per striation in $\theta(x)$.

However

$$\theta'_i(x) = \frac{-C}{k_0 a_i} \frac{[(x-x_i)^2/a_i^2 + 1]}{\sqrt{1 - \frac{(x-x_i)^2}{a_i^2}}}$$

also becomes infinite so the amplitude of the plane wave contribution goes to zero.

The rod profile is an extreme idealization of the sharpness of the edge of a striation. The fact that we will evaluate $\hat{U}(k)$ by a fast Fourier transform rather than analytically, means we are automatically smoothing the edges of the striation since the largest value of θ obtainable is

$$\frac{\phi_i(x = x_i + a_i - \Delta x) - \phi_i(x = x_i + a_i)}{k_0 \Delta x}$$

So $\theta_{i \max} \approx \frac{n_c}{n} \sqrt{\frac{2a_i}{\Delta x}}$ where Δx is the step size = L/N where $N = 2^m$ is the number of Fourier components (plane waves) to be determined.

We have carried out the analysis for $m = 14$ and 15 to see the impact on propagation effects of changing the step size and hence the maximum plane wave angle. The differences were negligible, indicating that for the cases we have treated, the largest angle of a significantly contributing plane wave was less than the largest angle obtainable by using $m = 15$. We do not know what this angle is for the rods. We estimate the angle for the Gaussian profile using previous analysis¹ which shows

$$\overline{\theta^2} = \frac{1}{(k_0 a_0)^2} \overline{\Delta\phi^2}$$

If we choose the restriction

$$d < \frac{L}{2\sqrt{\overline{\theta^2}}} = \frac{k_0 a_0 L}{2\Delta\phi_{\text{rms}}}$$

or

$$\lambda d < \frac{\pi a_0 L}{\Delta\phi_{\text{rms}}} \approx \frac{150}{\Delta\phi_{\text{rms}}}$$

we should be confident that the finiteness of the interval, L , will not impact the calculations. It turns out that the results of importance for this study occur well before this limit is reached.

The parameters λd and $\Delta\phi_{\text{rms}}$ (or C) uniquely determine the propagation effects for a given striation structure. This can be seen from an alternate expression for the signal previously obtained¹

$$U(x_0, d) = \sqrt{\frac{1}{i\lambda d}} \int dx e^{i[\Delta\phi(x) + \pi(x-x_0)^2/\lambda d]}$$

For a fixed structure, $\Delta\phi(x)$ and $\Delta\phi_{\text{rms}}$ are both linear in C and therefore scale together. The only other parameter in the integral is λd . We may therefore do all calculations at one frequency varying C and d , present the results in terms of λd and $\Delta\phi_{\text{rms}}$ and obtain results at other frequencies by scaling.

2.2 IMPLEMENTATION

We choose a range of λd of interest by considering the frequency range of interest to be 300 MHz to 30 GHz and the distance range of interest to be 10^2 to 10^4 km. This limits

$$10^{-3} \leq \lambda d \leq 10 \text{ km}^2.$$

We choose $\sqrt{0.1} \leq \Delta\phi_{\text{rms}} \leq 100$ radians. Effects are negligible at and below the lower limit. The higher limit is chosen so as to insure adequate sampling of $e^{i\phi(x)}$ by the fast Fourier transform. These limits are sufficient to demonstrate results. The transparency of the medium is assured for high altitude plasma by the restriction $\Delta\phi_{\text{rms}} \leq 100$ radians. For a temperature around 1000°K , the ion-electron momentum transfer collision frequency

$$\nu_{ei}(\text{s}^{-1}) \approx 10^{-3} n_e(\text{cm}^{-3}).$$

A wave traveling a thickness z of the plasma then suffers $\int_0^z dz 1.28 \cdot 10^{-11} n_e^2 \lambda^2$ dB of attenuation where λ is the wave length in km. For the 64 km width of the striations the average attenuation is

$$\bar{A} = \frac{1.28 \cdot 10^{-11} \lambda^2}{64} \int_0^L dx \int_0^z dz \sum_i n_i^2(x, z)$$

Now

$$\int_0^L dx \int_0^z dz n_0^2 e^{-2(\bar{x} - \bar{x}_i)^2 / a_i^2} = \frac{\pi n_0^2 a_i^2}{2}$$

for Gaussian profiles and

$$\int_0^L dx \int_0^z dz \begin{cases} n_0^2, & r < a_i \\ 0, & r > a_i \end{cases} = \pi n_0^2 a_i^2$$

for rods.

Therefore, the rods produce twice the average attenuation that Gaussian profiles produce for the same electron content. For Gaussian profiles we have

$$\bar{A} = 10^{-13} \lambda^2 n_0^2 \sum_i a_i^2$$

For the particular set of 210 striations we use

$$\sum_i a_i^2 = 112.62$$

and $\bar{A} = 3.54 \cdot 10^{-11} \lambda^2 n_0^2$ dB where λ is in km and n_0 is cm^{-3} . Similarly, we have

$$\Delta\phi_{\text{rms}} = 2.818 \cdot 10^{-3} \lambda n_0 Q_{\text{rms}}$$

where $Q(x) = \int_0^L \frac{n_e(x,z)}{n_0} dz$ is the normalized integrated electron density in km. For the particular set used, $Q_{\text{rms}} = 2.071$ km so $\Delta\phi_{\text{rms}} = 5.836 \cdot 10^{-3} \cdot n_0 = 98\sqrt{\bar{A}}$.

For $\Delta\phi_{\text{rms}} \leq 100$, $\bar{A} \leq 10^{-2}$ dB. For the rods, $Q_{\text{rms}} = 2.55$ km, so $\Delta\phi_{\text{rms}} = 7.186 \cdot 10^{-3} \lambda n_0$ but $\bar{A} = 7.08 \cdot 10^{-11} \lambda^2 n_0^2 = 1.37 \cdot 10^{-6} \frac{\Delta\phi_{\text{rms}}^2}{\lambda^2}$ and absorption is negligible for $\Delta\phi_{\text{rms}} \leq 100$. Our procedure is to obtain $Q(x)$ directly from the 210 striations in steps of $64 \text{ km}/2^{15} = 1.953 \text{ m}$ and store it. For each value of $\Delta\phi_{\text{rms}}$ desired we multiply $Q(x)$ by $\Delta\phi_{\text{rms}}/Q_{\text{rms}}$ to obtain $\phi(x)$ and

fast Fourier transform $e^{i\phi(x)}$ to obtain $U(k)$. We use the Berkeley computer library routine CFFT. Their write-up describes the inverse transform as

$$U(x,0) = \sum_{j=0}^{N-1} \hat{U}(j) e^{ik_j x}$$

where

$$k_j = \frac{2\pi j}{L}.$$

This reproduces the function $U(x,0)$ exactly at the sampled points $x_p = \frac{Lp}{N}$ $p = 0,1,2,\dots,N-1$. Unfortunately, it is not the appropriate inverse transform. The proper one for best fit to the function at all x is

$$U(x,0) = \sum_{j=0}^{N/2} \hat{U}(j) e^{ik_j x} + \sum_{j=1}^{N/2-1} \hat{U}(N-j) e^{-ik_j x}$$

which also reproduces the function exactly.

This is the proper truncation of the infinite Fourier series which has both positive and negative wave numbers. The one described in the Berkeley write-up replaced the negative wave numbers by wave numbers one period higher which introduces high frequency (wave number) content the original function did not have.

Having the $\hat{U}(j)$ for the specified $\Delta\phi_{rms}$, we then modify $U(j)$ for each of a set of values of λd to describe the wave a distance d away as

$$\hat{U}(j,d) = \hat{U}(j) e^{-ik_j^2 d \lambda / 4\pi} \quad j = 0, 1, \dots, N/2 ;$$

$$\hat{U}(N-j,d) = \hat{U}(N-j) e^{-ik_j^2 \lambda d / 4\pi} \quad j = 1, 2, \dots, N/2-1 .$$

and call the inverse CFFT to obtain $U(x,d)$. The routine performs the inverse transform properly.

For the rod profiles we redid the calculations using both 2^{14} and 2^{15} Fourier components and found the results consistent, signifying the sampling of $Q(x)$ to be adequate.

3. RESULTS

In this section we compare the propagation effects of rod profile striations and Gaussian striations. Since the computer routine calculates the signal at 2^{15} values of x over a 64 km range, we have a good sampling for statistics. The output of the routine includes the mean intensity, $\overline{|U|^2}$, which should be unity by conservation of energy (this check on the results was unity for all cases), and the scintillation index,

$$S_4 \equiv \sqrt{|U|^4 - 1}.$$

The distribution of the intensity is obtained by printing the number of samples in bins 3 dB wide. The following table has the percent of samples in each bin for those cases where at least 0.5% of the samples were less than -3 dB.

The columns begin with the percent less than -30 dB and work up in 3 dB increments with the last column for samples ≥ 12 dB. The T signifies a finite percentage less than or equal to .05. The calculations were carried out for λd up to the lesser of 10 and $100/\Delta\phi_{rms}$. We chose to stop the tabulation at λd the lesser of 10 and $10/\Delta\phi_{rms}$.

The results for Gaussian profiles do not enter the table for $\lambda d < (\Delta\phi_{rms})^{-1}$. The results for rod profiles do not enter the table for $\lambda d < 10^{-1/2}(\Delta\phi_{rms})^{-2}$ within the range of λd of interest.

If one considers the question of how one scales a critical quantity with wave length, one will get different scaling for the rod and Gaussian profiles. For example, consider the value of on-axis electron density, n_0 , below which more than 99.5% of the signal is above -3 dB. For the Gaussian

$\log_{10} \frac{1}{\sigma_{rms}}$		$\log_{10} d$	<-30	-27	-24	-21	-18	-15	-12	-9	-6	-3	0	3	6	9	12	>12
r	g	-5									0	3.3	52.5	43.4	0.8	0		
		1								0	1.6	8.8	40.5	48.7	0.4	0		
r	g	0								0	0.7	7.2	39.3	52.9	0			
		-5								0	0.2	5.3	51.5	41.6	1.3	0		
r	g	0	T	T	T	T	T	0.1	0.4	1.2	3.4	14.5	39.8	32.1	8.0	0.2	0	
		5	T	T	0.1	0.2	0.3	1.0	1.5	5.0	11.1	16.2	23.6	27.9	12.9	0.3	0	
r	g	1	T	T	0.1	0.4	0.6	1.2	2.6	4.0	7.8	13.1	29.2	28.8	11.9	0.3	0	
		5	T	T	0.1	0.5	0.8	2.2	2.2	3.3	6.8	13.3	26.8	33.2	9.8	0.3	0	
r	g	1.5						0	T	0.1	3.0	55.2	40.2	1.5	0			
		-1	T	T	T	T	T	0.1	0.9	3.0	13.3	43.1	32.5	6.7	0.2	0		
r	g	-1.5	T	T	0.1	0.2	0.6	0.9	1.8	3.6	8.6	17.3	28.6	26.4	10.8	1.2	0	
		0	0.1	0.1	0.2	0.3	0.8	1.7	2.7	4.0	9.3	17.0	24.5	27.5	10.4	1.5	0	
r	g	5	0.1	0.1	0.2	0.3	0.6	1.1	1.8	5.0	13.0	18.9	23.0	22.4	11.5	2.5	0	
		5	0.1	0.1	0.2	0.5	0.8	1.4	2.4	5.3	8.9	16.5	25.2	27.2	10.5	1.2	0	
r	g	1				0	T	T	T	T	0.2	2.9	59.2	36.0	1.6	0		
		-2.5	T	T	T	T	T	0.1	0.1	0.4	1.9	9.7	49.6	32.9	5.1	0.1	0	
r	g	-2	T	T	0.1	0.1	0.3	0.6	1.3	2.9	6.0	16.7	34.4	27.3	9.5	0.8	0	
		-1.5	0.1	0.1	0.2	0.3	0.7	1.4	2.7	5.5	10.3	18.0	24.3	23.6	10.8	2.0	T	0
r	g	-1	0.1	0.1	0.2	0.3	0.7	1.4	2.7	5.5	10.3	18.0	24.3	23.6	10.8	2.0	T	0
		5	0.1	0.1	0.3	0.5	0.8	1.7	3.1	5.6	10.5	17.1	23.5	22.5	11.8	2.2	T	0
r	g	0	0.1	0.1	0.2	0.4	0.9	1.9	3.4	5.9	11.1	16.8	23.1	22.1	11.9	2.2	0	
		5	0.1	0.1	0.2	0.5	0.7	1.3	2.9	5.4	10.2	18.2	23.7	23.0	12.2	1.6	0	
r	g	1.5	0	T	T	T	T	0.1	0.3	0.7	2.0	5.6	57.0	29.0	5.6	0.2	0	
		-3	T	T	T	0.1	0.2	0.4	0.8	1.8	3.9	10.1	46.1	28.4	7.5	0.5	T	0
r	g	-2.5	0.1	0.1	0.1	0.2	0.5	1.0	1.9	3.5	7.2	16.5	31.6	26.1	10.0	1.3	T	0
		-2	0.1	0.1	0.2	0.4	0.7	1.6	2.9	5.5	10.1	17.0	23.9	24.1	11.7	1.7	T	0
r	g	-1.5	0.1	0.1	0.2	0.4	0.7	1.6	2.9	5.5	10.1	17.0	23.9	24.1	11.7	1.7	T	0
		0	0.1	0.1	0.2	0.4	0.8	1.6	3.0	5.6	10.3	17.1	23.5	23.6	11.8	1.6	0.1	0
r	g	-1	0.1	0.1	0.2	0.4	0.8	1.6	3.0	5.6	10.3	17.1	23.5	23.6	11.8	1.6	0.1	0
		5	0.1	0.1	0.2	0.4	0.7	1.6	3.1	5.9	10.5	17.3	23.7	23.2	11.5	1.9	T	0
r	g	0	0.1	0.1	0.2	0.4	0.7	1.6	3.1	5.9	10.5	17.3	23.7	23.4	11.2	2.3	0.1	0
		5	0.1	0.1	0.2	0.4	0.8	1.7	3.2	7.8	11.7	17.3	22.0	21.2	10.6	2.6	0.2	0
r	g	2																
		-3	T	T	T	0.1	0.1	0.3	0.7	1.4	3.6	11.4	46.0	29.0	6.8	0.5	T	0
r	g	-2.5	T	T	0.1	0.2	0.4	0.6	1.6	3.2	7.3	16.7	32.2	27.0	9.4	1.1	T	0
		-2	0.1	0.1	0.1	0.4	0.7	1.4	2.8	5.4	10.2	17.5	24.9	23.3	11.0	2.0	0.1	0
r	g	-1.5	0.1	0.1	0.2	0.4	0.8	1.6	3.3	6.0	10.1	17.1	23.9	22.7	11.7	2.0	T	0
		0	0.1	0.1	0.2	0.4	0.8	1.6	3.3	6.0	10.1	17.1	23.9	22.7	11.7	2.0	T	0
r	g	5	0.1	0.1	0.2	0.4	0.8	1.6	3.3	6.0	10.1	17.1	23.9	22.7	11.7	2.0	T	0
		5	0.1	0.1	0.2	0.4	0.8	1.6	3.3	6.0	10.1	17.1	23.9	22.7	11.7	2.0	T	0

profile,

$$\Delta\phi_{rms}\lambda d = 1 = r_e \lambda^2 n_0 d Q_{rms}$$

and n_0 scales as λ^{-2} for a given structure and d . For the rod profiles,

$$(\Delta\phi_{rms})^2 \lambda d = 10^{-1/2} = r_e^2 \lambda^3 n_0^2 d Q_{rms}$$

and n_0 scales as $\lambda^{-3/2}$ for a given structure and d .

Therefore, the important question of the payoff of higher frequencies is bounded by the λ^{-2} and $\lambda^{-3/2}$ scaling for Gaussian and rod profiles. Earlier work⁴ by Mission Research Corporation (MRC) had suggested that propagation effects depended on $\Delta\phi_{rms}$ alone, which means n_0 scales as λ^{-1} . This is because their analysis assumed $\lambda d \gg 1$.

We illustrate this difference by including in the output the average bit error probability, \bar{P}_e , for noncoherent frequency shift key (FSK) modulation according to MRC's formula⁴,

$$\bar{P}_e = \int_0^\infty P(\gamma) P_e(\gamma) d\gamma$$

where $P(\cdot)$ is the probability density that the signal to noise ratio, (S/N), is γ and $P_e(\gamma) = \frac{1}{2} e^{-\gamma/2}$ is the bit error probability for a given (S/N) of γ . If γ_0 is the (S/N) in the absence of the striations then we use $\gamma = \gamma_0 |U_i|^2$ and

$$\int_0^\infty P_e(\gamma) P(\gamma) d\gamma = \frac{1}{N} \sum_{i=1}^N P_e(\gamma_0 |U_i|^2) = \bar{P}_e$$

where the sum is over the $N = 2^{15}$ values of x . We illustrate the results in Figure 3, where the line labeled MRC is from their report. The case chosen is for $\gamma_0 = 31.623$ (15 dB). The bracketed lines near MRC's curve show our results for $\lambda d = 10 \text{ km}^2$. The brackets signify the spread between rod(r) and Gaussian(g) profiles. We approach the MRC result at the high limit of λd . To the right of the MRC curve are three lines signifying the results for $\lambda d = 0.1(r)$, $\lambda d = 0.1(g)$ and $\lambda d = 0.01(g)$. Sprinkled in between are various other points for other cases. It is apparent that at lower values of λd , $\overline{P_e}$ gets better faster for Gaussian than rod profiles. The best way to present results of this type is on a λd versus $\Delta\phi_{\text{rms}}$ plane. We demonstrate for two contours of $\overline{P_e} = 10^{-4}$ and 10^{-2} in Figure 4. The mesh points are the cases we have run. We sketch the contours so they are on the correct side of the mesh point values.

The utility of the λd - $\Delta\phi_{\text{rms}}$ chart is apparent for putting the system-effect problem in perspective. Since $10^{2.5} \leq d \leq 10^{3.5}$, in general we see that UHF($\lambda=10^{-3}$) lies in a band at the top where trouble begins in the region $0.3 < \Delta\phi < 1$ for both profiles. S Band($\lambda=10^{-4}$) is below this band where trouble begins in the region $1 < \Delta\phi_{\text{rms}} < 3$ for rods and $3 < \Delta\phi_{\text{rms}} < 20$ for Gaussian profiles. Finally, K Band($\lambda=10^{-5}$) is below this band with $3 < \Delta\phi_{\text{rms}} < 10$ for rods and $20 < \Delta\phi_{\text{rms}} < 100$ for the Gaussian profiles. Thus, the highest frequencies are the most affected by uncertainties in the profile form.

This chart was used by researchers in an attempt to put the measured scintillation index in perspective. We sketch contours of S_4 for Gaussian and rod profiles in Figures 5 and 6. The Gaussian profiles give rise to large focusing effects which lead to large values of S_4 in the focal region mentioned in previous work¹. From the table we saw that only Gaussian profiles produced

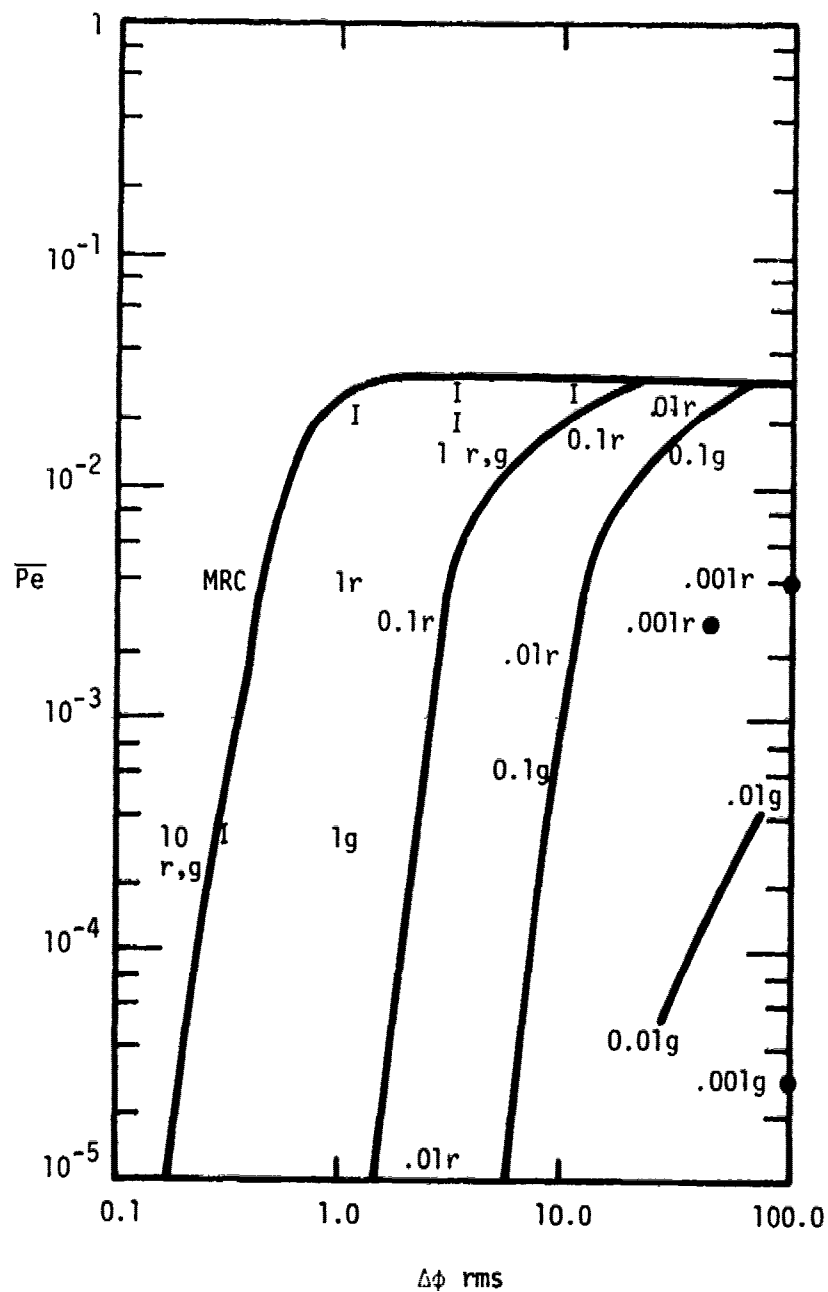


FIGURE 3 - Average Bit Error Probability Versus rms Phase Fluctuation for Noncoherent FSK Modulation and 15db Average Signal-to-Noise Ratio

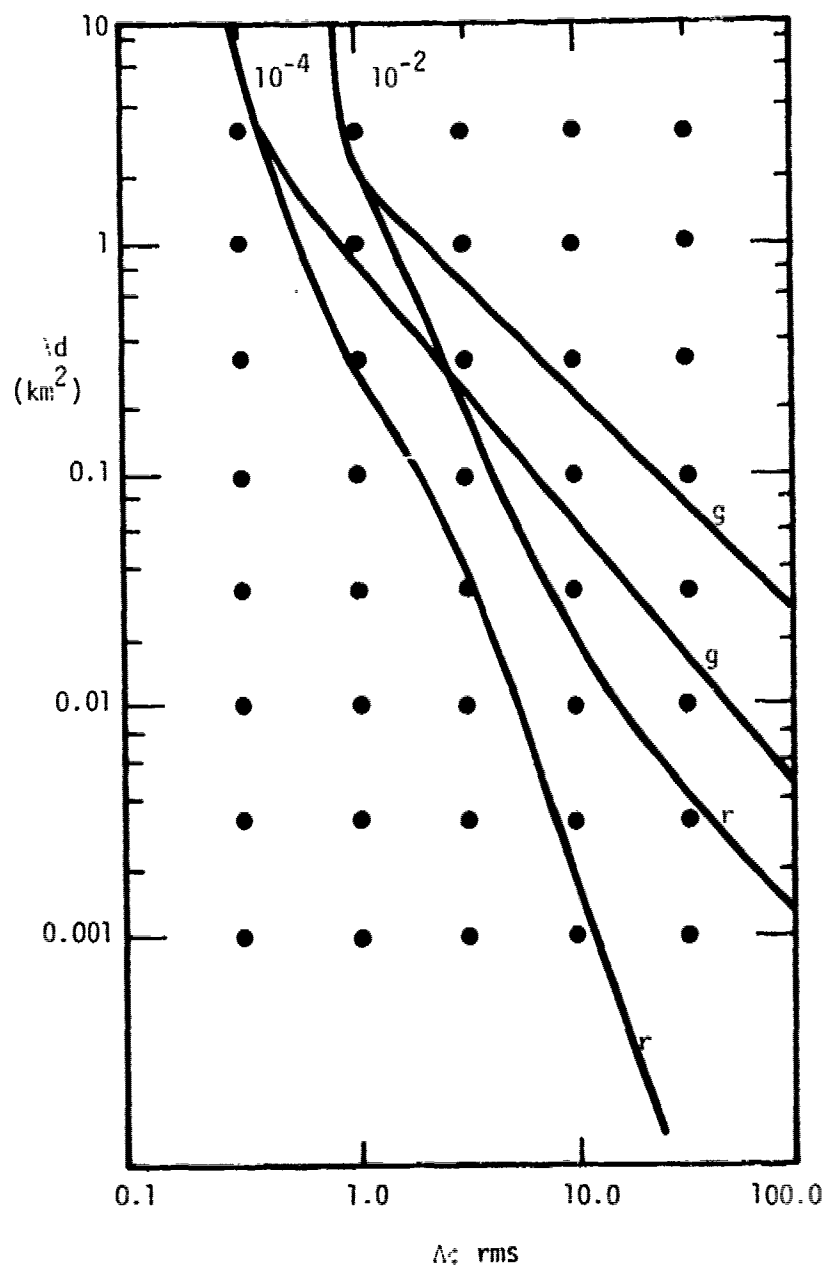


FIGURE 4 - Contours of Bit Error Probability

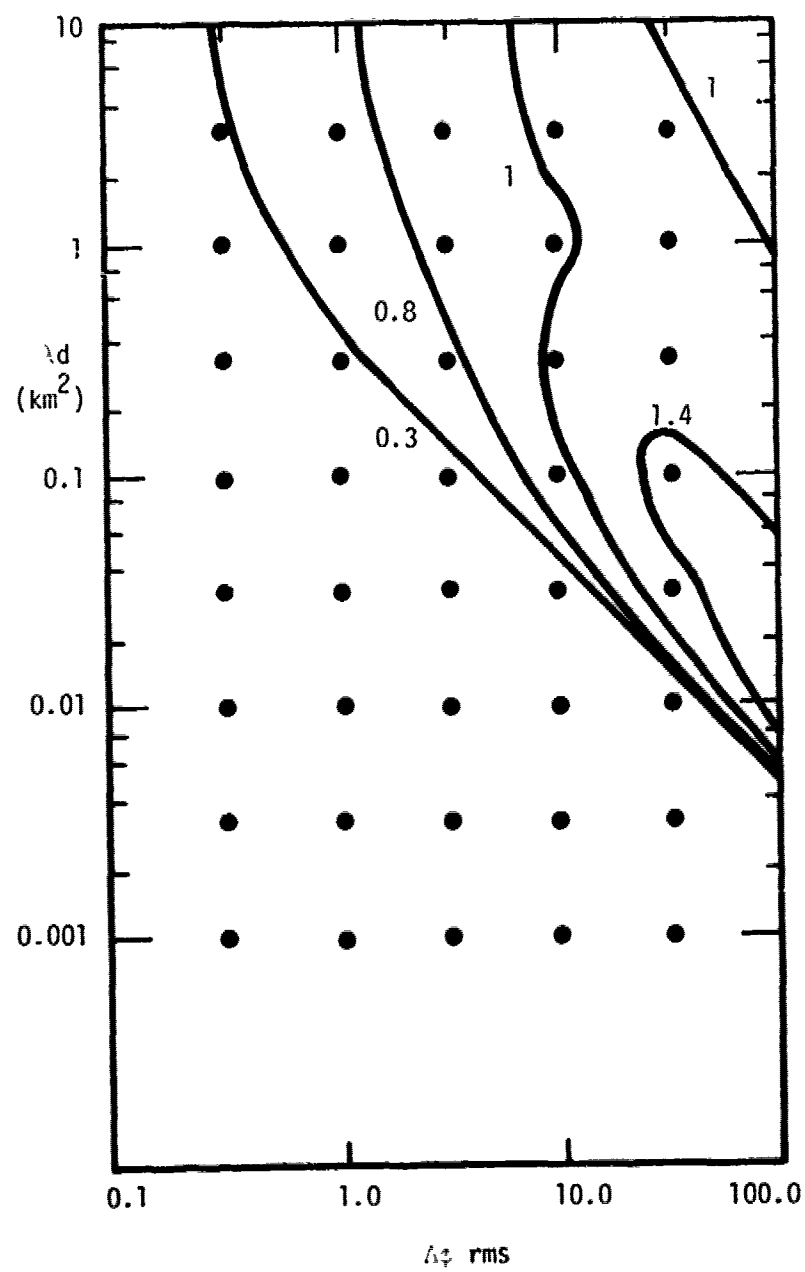


FIGURE 5 - Contours of S_4 ; Gaussian

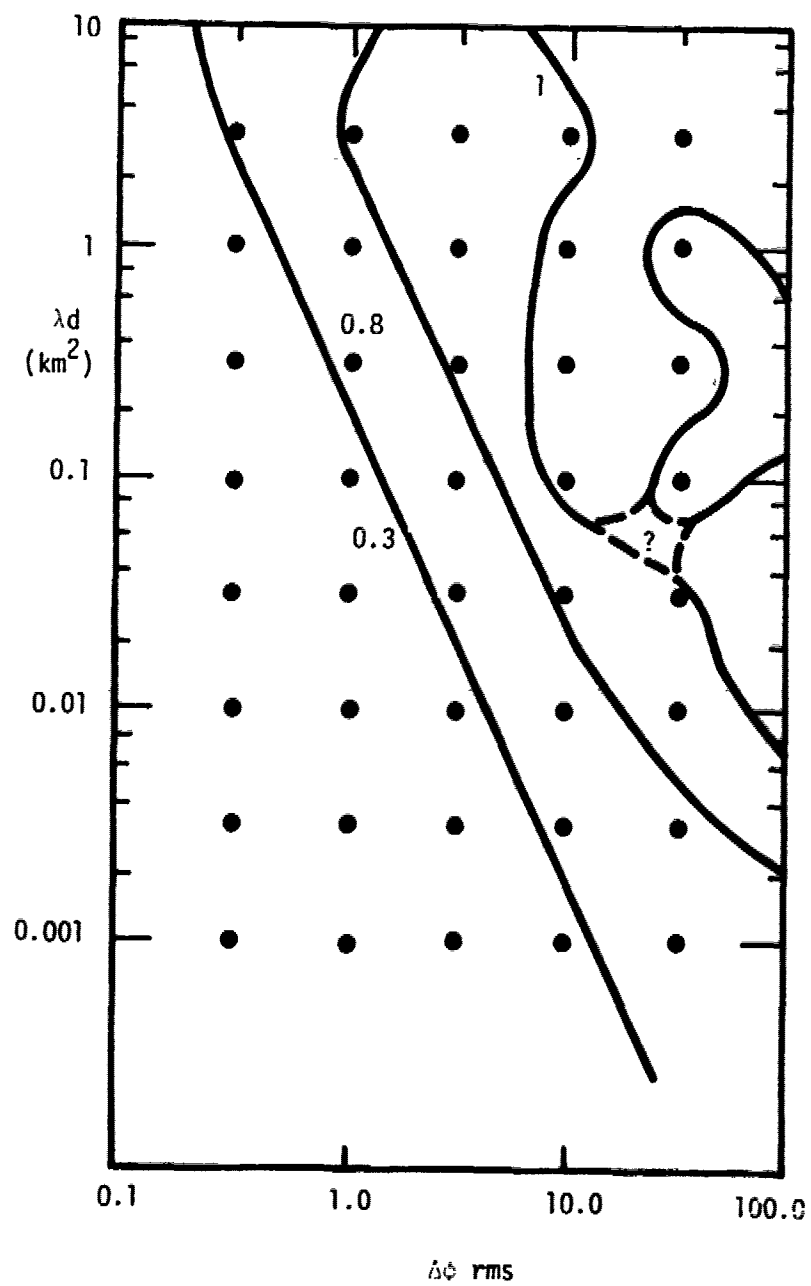


FIGURE 6 - Contours of S_4 ; Rod

signals ≥ 12 dB. The rod profiles do not give rise to high values of S_4 , and there does not seem to be any consistency as to which values are above or below 1 as can be seen by the uncertainty in drawing the $S_4 = 1$ contour in Figure 6.

We believe S_4 should be abandoned as a measure of the severity of propagation effects since it is influenced by intensity peaks which are unimportant for degradation. Comparisons of Figures 4, 5 and 6 show correlation of the onset of trouble ($\overline{P_e} = 10^{-4}$ and $S_4 = 0.3$) but we should have a better measure of the degree of trouble. As an example, we show in Figure 7 the contour for 1% probability of fades > 12 dB for rod and Gaussian profiles. Here, the separate scaling is apparent. The correlation of this contour with the $S_4 = 0.8$ contour of Figure 6 is not bad for a small range, but the correlation with S_4 in Figure 5 for the Gaussian profiles is non-existent.

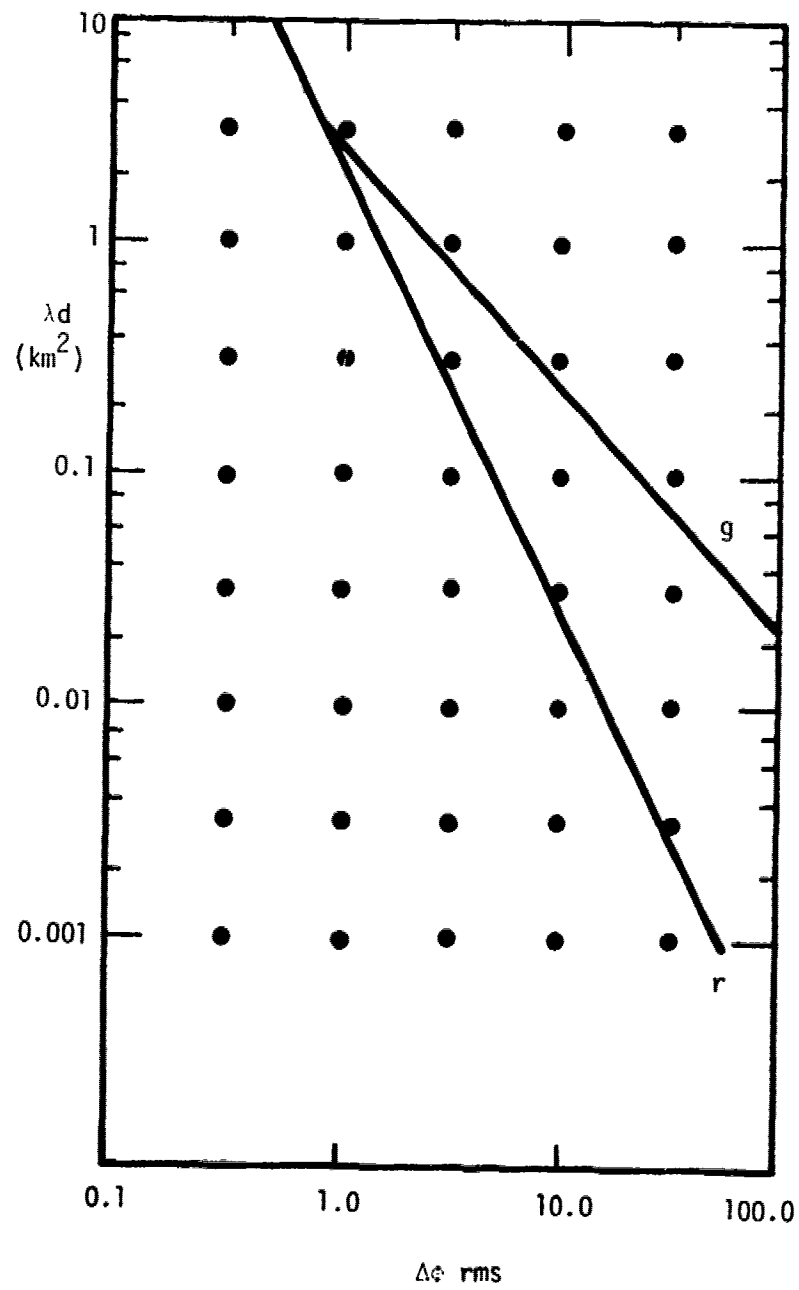


FIGURE 7 - Contours for 1% Probability of Fades > 12dB

REFERENCES

1. Sachs, David L., "Propagation Effects of Large Phase Variations in a Striated Plasma", DNA 3852T, October 1975.
2. Rino, C.L. and D.L. Sachs, "Striation Models for High Altitude Nuclear Propagation Effects", Stanford Research Institute (to be published).
3. Price, Gary, Walter Chesnut and Alan Burns, Stanford Research Institute, April, 1972.
4. Carron, N.J., Mission Research Corporation, February 1975.

DISTRIBUTION LIST

DEPARTMENT OF DEFENSE

Director
Command Control Technical Center
ATTN: C-312, R. Mason
ATTN: C-650, G. C. Jones
ATTN: C-650, W. Heidig

Director
Defense Advanced Resch Proj Agency
ATTN: Nuclear Monitoring Research
ATTN: Strategic Tech. Office

Defense Communication Engineer Center
ATTN: Code R520, R. L. Crawford
ATTN: Code R410, James W. McLean

Director
Defense Communications Agency
ATTN: Code 480
ATTN: Code S10, R. W. Rostron

Defense Documentation Center
12 cy ATTN: TC

Director
Defense Intelligence Agency
ATTN: W. Wiliig, DC-7D
ATTN: DT-1B

Director
Defense Nuclear Agency
ATTN: STSI, Archives
ATTN: STVL
ATTN: DDST
3 cy ATTN: STTL, Tech. Library
3 cy ATTN: RAAE

Dir. of Defense Resch. & Engineering
ATTN: DD/S&SS, John B. Walsh

Commander
Field Command
Defense Nuclear Agency
ATTN: FCPR

Director
Interservice Nuclear Weapons School
ATTN: Document Control

Director
Joint Strat. Tgt. Planning Staff, JCS
ATTN: JLTW-2
ATTN: JPST, Captain G. D. Goetz

Chief
Livermore Division, Fld. Command DNA
Lawrence Livermore Laboratory
ATTN: FCPRL

Director
National Security Agency
ATTN: Frank Leonard
ATTN: W14, Pat Clark
ATTN: John Skillman, R52

DEPARTMENT OF DEFENSE (Continued)

OJCS/J-3
ATTN: WWMCCS, Eval. Ofc., Mr. Toma

Director
Telecommunications & Comd. & Con. Sys.
ATTN: Asst. Dir. (SYS)
ATTN: Scientific Advisor

DEPARTMENT OF THE ARMY

Commander/Director
Atmospheric Sciences Laboratory
ATTN: DRSEL-BL-SY-S, F. E. Niles

Chief C-E Services Division
US Army Communications Cnd.
ATTN: CC-OPS-CE

Commander
Harry Diamond Laboratories
ATTN: DRXDO-NP, Francis N. Wimenitz
ATTN: DRXDO-RB, Robert Williams
ATTN: Mildred H. Weiner, DRXDO-TI
ATTN: DRXDO-NP, Cyrus Mgazed

Commander
TRASANA
ATTN: TCC/F. Payan, Jr.
ATTN: EAB

Commander
U.S. Army Comm-Elec Engr. Instal. Agy.
ATTN: EED-PED, George Lane
ATTN: EED-PED, Ward Nair

Commander
U.S. Army Electronics Command
ATTN: DRSEL-PL-ENV, Hans A. Bomke

Commander
U.S. Army Foreign Science & Tech. Ctr.
ATTN: P. A. Crowley
ATTN: R. Jones

Commander
U.S. Army Materiel Dev. & Readiness Cnd.
ATTN: DRCLDC, J. A. Bender
ATTN: DRUDE-D, Lawrence Flynn

Commander
U.S. Army Missile Command
ATTN: DRSMI-YTT, W. G. Preussel, Jr.

Commander
U.S. Army Nuclear Agency
ATTN: MONA-WE, J. Berberet

DEPARTMENT OF THE NAVY

Chief of Naval Research
ATTN: Code 464, Jacob L. Warner
ATTN: Code 464, Thomas P. Quinn

DEPARTMENT OF THE NAVY (Continued)

Commander
Naval Air Systems Command
ATTN: AIR 5381

Commander
Naval Electronic Systems Command
Naval Electronic Systems Cmd. Hqs.
ATTN: John E. DonCarlos
ATTN: PME 117
ATTN: PME 117-T, Satellite Comm. Project Off.
ATTN: NAVALEX 034, T. Barry Hughes

Commander
Naval Electronics Laboratory Center
ATTN: R. Eastman
ATTN: Code 0230, C. Baggett
ATTN: William F. Moler
3 cy ATTN: Code 2200

Commanding Officer
Naval Intelligence Support Ctr.
ATTN: Mr. Dubbin, STIC 12

Director
Naval Research Laboratory
ATTN: Hdq. Comm. Dir., Bruce Wald
ATTN: Code 7700, Timothy P. Coffey
ATTN: Code 5460, Radio Electromag. Prop. Br.
ATTN: Code 5430
3 cy ATTN: Code 7701, Jack D. Brown

Commander
Naval Space Surveillance System
ATTN: CAPT J. H. Burton

Commander
Naval Surface Weapons Center
ATTN: Code WA501, Navy Nuc. Prgms. Off.

Director
Strategic Systems Project Office
ATTN: NSP-2141

DEPARTMENT OF THE AIR FORCE

Commander
ADC/DC
ATTN: DC, Mr. Long

Commander
ADCOM/XPD
ATTN: XPQDQ

AF Geophysics Laboratory, AFSC
ATTN: SUOL, AFRL. Rsch. Lib.
ATTN: OPR, James C. Ulwick
ATTN: LKB, Kenneth S. W. Champion
ATTN: OPR, Alva T. Stair

AF Weapons Laboratory, AFSC
ATTN: DYT, Capt L. Wittwer
ATTN: SAS, John M. Kamm
ATTN: SUL

AFTAC
ATTN: TF/Maj Wiley
ATTN: TN

DEPARTMENT OF THE AIR FORCE (Continued)

Air Force Avionics Laboratory, AFSC
ATTN: AAD, Wade Hunt
ATTN: AFAL, AAB, H. M. Hartman

Headquarters
Electronic Systems Division, (AFSC)
ATTN: YSEV
ATTN: Lt Col J. Morin, CDEI, XRC
ATTN: Lt Michaels, XRE

Commander
Foreign Technology Division, AFSC
ATTN: TD-BTA, Library

HQ USAF/RD
ATTN: RDQ

Commander
Rome Air Development Center, AFSC
ATTN: EMTLD, Doc. Lib.
ATTN: ETE, A. Lorentzen

SAMSO/SZ
ATTN: SZJ, Major Lawrence Doan

Commander in Chief
Strategic Air Command
ATTN: XPFS, Maj Brian G. Stephan
ATTN: ADOP, Capt Bruce Bauer

ENERGY RESEARCH & DEVELOPMENT ADMINISTRATION

University of California
Lawrence Livermore Laboratory
ATTN: Tech. Info., Dept. 1-3

Los Alamos Scientific Laboratory
ATTN: Doc. Con. for R. F. Tasehek

Sandia Laboratories
ATTN: Doc. Con. for W. D. Brown
ATTN: Doc. Con. for D. A. Dahlgren, Org. 1722
ATTN: Doc. Con. for J. P. Martin, Org. 1732
ATTN: Doc. Con. for A. Dean Thornbrough

OTHER GOVERNMENT AGENCIES

Department of Commerce
Office of Telecommunications
ATTN: G. Reed
ATTN: William F. Utlaut
ATTN: L. A. Berry

National Oceanic & Atmospheric Admin.
Environmental Research Laboratories
ATTN: Joseph H. Pope
ATTN: C. L. Retenach

DEPARTMENT OF DEFENSE CONTRACTORS

Aeronutronic Ford Corporation
Western Development Laboratories Div.
ATTN: J. T. Mattingley, MS X22

DEPARTMENT OF DEFENSE CONTRACTORS (Continued)

Acrospace Corporation
ATTN: S. P. Bower
ATTN: Irving M. Garfunkel
ATTN: SMFA for PWV
ATTN: T. M. Salm
ATTN: V. Josephson

Analytical Systems Engineering Corp.
ATTN: Radio Sciences

The Boeing Company
ATTN: D. Murray
ATTN: Glen Keister

Univ. of California at San Diego
ATTN: Henry G. Booker

Calspan Corporation
ATTN: Romeo A. Delibonis

Computer Sciences Corporation
ATTN: John Spoor
ATTN: H. Blank

Comsat Laboratories
ATTN: R. R. Taur

Cornell University
Department of Electrical Engineering
ATTN: D. T. Farley, Jr.

ESL, Inc.
ATTN: James Marshall
ATTN: J. Roberts
ATTN: V. L. Mower
ATTN: R. K. Stevens

General Electric Company
TEMPO-Center for Advanced Studies
ATTN: Don Chandler
ATTN: DASLAC

General Electric Company
ATTN: F. A. Reibert

General Research Corporation
ATTN: John Ise, Jr.

Geophysical Institute
University of Alaska
ATTN: Neal Brown
ATTN: T. N. Davis
ATTN: Tech. Lib.

GTE Sylvania, Inc.
Electronics Systems Grp-Eastern Div.
ATTN: Marshal Cross

HRB-Singer, Inc.
ATTN: Larry Feathers

University of Illinois
Department of Electrical Engineering
ATTN: K. C. Yeh

DEPARTMENT OF DEFENSE CONTRACTORS (Continued)

Institute for Defense Analyses
ATTN: Ernest Bauer
ATTN: Hans Wolfhard
ATTN: J. M. Aern
ATTN: Joel Bengston

Intl. Tel. & Telegraph Corporation
ATTN: Tech. Lib.

Johns Hopkins University
Applied Physics Laboratory
ATTN: Document Librarian

Lockheed Missiles & Space Co., Inc.
ATTN: Dept. 60-12

Lockheed Missiles and Space Company
ATTN: Billy M. McCormac, Dept. 52-54
ATTN: Martin Walt, Dept. 52-10
ATTN: Richard G. Johnson, Dept. 52-12

M.I.T. Lincoln Laboratory
ATTN: Mr. Walden, X113
ATTN: Lib. A-082 for David M. Towle
ATTN: D. Clark
ATTN: James H. Pannell, L-246

Martin Marietta Corporation
Denver Division
ATTN: Special Projects Program 248

Maxwell Laboratories, Inc.
ATTN: A. J. Shannon
ATTN: Victor Fargo
ATTN: A. N. Rostocker

McDonnell Douglas Corporation
ATTN: J. Moule
ATTN: N. Harris

Mission Research Corporation
ATTN: R. Hendrick
ATTN: M. Scheibe
ATTN: R. Bogusch
ATTN: Steven L. Gutsche
ATTN: P. Fischer
ATTN: Dave Sowle

The Mitre Corporation
ATTN: S. A. Morin, M/S
ATTN: C. E. Callahan
ATTN: J. C. Keenan
ATTN: Chief Scientist, W. Sen
ATTN: G. Harding

The Mitre Corporation
ATTN: Allen Schneider

Pacific-Sierra Research Corp.
ATTN: E. C. Field, Jr.

Photometrics, Inc.
ATTN: Irving L. Kofsky

Physical Dynamics, Inc.
ATTN: A. Thompson
ATTN: Joseph B. Workman

DEPARTMENT OF DEFENSE CONTRACTORS (Continued)

R & D Associates

ATTN: Bryan Gabbard
ATTN: Richard Latter
ATTN: William B. Wright, Jr.
ATTN: Robert E. LeLevier

3 cy ATTN: Forrest Gilmore

The Rand Corporation

ATTN: Cullen Crain

Science Applications, Inc.

ATTN: E. A. Straker
ATTN: D. Sachs
ATTN: Lewis M. Linson

Science Applications, Inc.
Huntsville Division

ATTN: Dale H. Divis

Science Applications, Incorporated

ATTN: B. Adams

DEPARTMENT OF DEFENSE CONTRACTORS (Continued)

Stanford Research Institute

ATTN: Charles L. Rino
ATTN: G. Smith
ATTN: David A. Johnson
ATTN: Donald Neilson
ATTN: Alan Burns
ATTN: Walter Jaye
ATTN: Walter G. Chesnut
ATTN: L. L. Cobb
ATTN: E. J. Fremouw

System Development Corporation

ATTN: E. G. Meyer

Tri-Com, Inc.

ATTN: Darrel Murray

TRW Systems Group

ATTN: R. K. Plebuch
ATTN: Robert M. Webb, M S R1-1150